RSC Advances

RSC Publishing

PAPER

View Article Online
View Journal | View Issue

Cite this: *RSC Adv.*, 2013, **3**, 24430

A facile approach to fabrication of well-dispersed NiO–ZnO composite hollow microspheres†

Qingshui Xie, Huizhang Guo, Xiangxin Zhang, Aolin Lu, Deqian Zeng, Yuanzhi Chen and Dong-Liang Peng*

Received 16th July 2013
Accepted 10th October 2013

DOI: 10.1039/c3ra43678k

www.rsc.org/advances

A novel, facile and template-free approach was developed for the fabrication of amorphous zinc-nickel citrate hollow microspheres and crystalline well-dispersed NiO–ZnO composite hollow microspheres. In this approach, amorphous zinc-nickel citrate hollow microspheres were prepared through a simple chemical reaction and with room temperature ageing at nickel nitrate solution. The zinc-nickel citrate hollow microspheres have an average size of about 1.4 μm. The average thickness of the shell is about 300 nm. The content of Ni in the zinc-nickel citrate can be simply adjusted by changing the ageing time. The well-dispersed NiO–ZnO composite hollow microspheres can be prepared *via* the perfect morphology inheritance of the zinc-nickel citrate hollow microspheres, by calcination at 500 °C for 2 h. The optical absorption of the samples can extend into the visible region after the loading of NiO. The NiO–ZnO composite hollow microspheres with the high content of NiO exhibit the highest photocatalytic activity for the degradation of different organic dyes including Rhodamine-B, methylene blue and methyl orange under UV irradiation, which might be ascribed to their highest separation efficiency of photogenerated electron–hole pairs. In addition, these NiO–ZnO composite photocatalysts can be used repeatedly without a significant decrease of the photocatalytic activity under UV irradiation.

Introduction

Recently, hollow micro/nanostructures with low density, high specific surface area and superior permeation have received considerable interest due to their unique physical and chemical properties and their potential applications in catalysis, drug delivery, gas sensing and energy storage.[1–6] Hitherto, many strategies have been developed to fabricate various hollow micro/nanostructures during the past few decades.[7–16] Unfortunately, most of researches focus on the control of the shape and interior void space of single oxide, the successful preparation of well-dispersed binary oxide composite hollow micro/nanostructures has rarely been reported due to the complicated procedures and severe reaction conditions. In general, the performances of the binary composites made up of different materials cannot be deemed as a simple superposition of the properties of individual counterparts due to the strong interfacial interactions between the different components.[17–19] Namely, the binary composites are expected to gain novel physical and/or chemical properties through the synergistic effect. For example, TiO_2–ZnO composite hollow microspheres have been successfully prepared, which show significant higher photocatalytic efficiency than pure ZnO evaluated under the same conditions.[20] However, the development of simple and template-free routes for fabricating well-dispersed metal oxide composite hollow structures still remains a great challenge.

ZnO is an attractive semiconductor with a direct wide band gap of 3.37 eV. Due to the high photocatalytic activity, high quantum efficiency, nontoxic nature and low cost, various morphologies of ZnO, such as nanotubes, flower-like nanoarchitectures and nanowires, have been successfully fabricated and used in photocatalysis area.[21–27] However, the fast recombination rate of the photogenerated electron–hole pairs limits their practical application. It has been demonstrated that the coupling of two different semiconductors with different energy levels causes a rapid separation of photogenerated electron–hole pairs and consequently increases the photocatalytic activity.[28–32] Nickel oxide (NiO) is a transparent semiconductor oxide with p-type conductivity and has been widely used in catalysis, battery cathodes, electrochromic films, chemical sensors and photovoltaic devices.[33–36] When coupled with ZnO, NiO would have some special advantages, such as low lattice mismatch with ZnO, high hole mobility and high p-type concentration, which is beneficial for the interaction between ZnO and NiO.[37–39] When the NiO–ZnO composite photocatalyst is irradiated by ultraviolet (UV) light, the photogenerated electrons and holes would migrate between NiO and ZnO. As a result, the photogenerated electron–hole pairs were effectively separated, which facilitates to enhance their photocatalytic activity. However, the successful preparation of

Department of Materials Science and Engineering, College of Materials, Fujian Key Laboratory of Advanced Materials, Xiamen University, Xiamen 361005, China

† Electronic supplementary information (ESI) available. See DOI: 10.1039/c3ra43678k

well-dispersed NiO–ZnO composite hollow microspheres, which are supposed to possess enhanced photocatalytic activity, has not been reported so far.

In this article, a novel, facile and template-free approach to fabricate amorphous zinc-nickel citrate hollow microspheres and crystalline NiO–ZnO composite hollow microspheres is reported. The content of Ni in the zinc-nickel citrate can be regulated simply by controlling the ageing time for the reaction solution. By calcining the as-obtained zinc-nickel citrate hollow microspheres at 500 °C for 2 h, the well-dispersed NiO–ZnO composite hollow microspheres were produced *via* perfect morphology inheritance. To the best of our knowledge, this is the first successful synthesis of the well-dispersed NiO–ZnO composite hollow microspheres. The resulting composite hollow microspheres exhibit visible-light absorption, greatly enhanced photocatalytic efficiency and good recyclability for the degradation of different organic dyes including Rhodamine-B (RhB), methylene blue (MB) and methyl orange (MO). The present method provides an excellent electric contact at the NiO–ZnO interface, which is beneficial for the transfer of photogenerated charge carriers between ZnO and NiO, leading to the decrease of the recombination rate of photogenerated electron–hole pairs and consequent enhancement of photocatalytic activity.

Experimental

Synthesis

In a typical procedure, amorphous zinc citrate hollow microspheres were synthesized through a facile and template-free route under mild conditions as described in our previous paper.[40] Newly prepared zinc citrate hollow microspheres (0.06 g) were dispersed in a certain concentration of nickel nitrate solution (30 mL) with the aid of ultrasonication. After ultrasonic dispersion for 10 min, the resulting suspension was aged for 6 h at room temperature. The resultant zinc-nickel citrate hollow microspheres were harvested by centrifugation and washed with distilled water for several times and then dried at 60 °C for 10 h. Finally, NiO–ZnO composite hollow microspheres were produced by the calcination of zinc-nickel citrate at 500 °C for 2 h in air.

Characterization

X-ray diffraction (XRD) measurements were carried out using a PANalytical X'pert PRO X-ray diffractometer with Cu Kα radiation (40 kV, 60 mA). Scanning electron microscopy (SEM) analysis was performed with a LEO-1530 field-emission scanning electron microscope equipped with an energy dispersive X-ray spectrometer. Transmission electron microscopy (TEM) observations were conducted using a JEM-2100 electron microscope operating at 200 kV. The thermogravimetric (TG) analysis was recorded on a Du Pont Instrument 1090B thermal analyzer. Fourier-transform infrared (FTIR) spectra were performed on a Nicolet Nexus-670 FT-IR spectrometer. X-Ray photoelectron spectroscopy (XPS) measurements were conducted using a PHI QUANTUM 2000 with a monochromatic Al K X-ray source (Thermo VG Scientific). UV-vis diffuse reflectance (DR) spectroscopy of the samples was performed using a Cary 500 UV-vis-NIR spectrophotometer. The room temperature photoluminescence (PL) of the samples were detected on a FLS-920T fluorescence spectrophotometer using an excitation wavelength of 325 nm from Xe 900 (450 W xenon arc lamp) as the light source.

Photocatalytic measurements

The photocatalytic properties of NiO–ZnO composite hollow microspheres with different content of NiO were evaluated by adding the known weight of the as-obtained samples into 200 mL of the known concentration of different organic dyes solution including RhB, MB and MO under the irradiation of a 300 W ultraviolet (UV) lamps (maximum emission at 253 nm). Prior to irradiation the suspension were stirred in the dark for 30 min to ensure the adsorption–desorption equilibrium between the catalyst and the dye. A comparative experiment in the absence of photocatalyst during UV irradiation was carried out. Samples exposed to the UV irradiation for different time intervals were taken out from the reaction suspension, centrifuged at 8000 rpm for 10 min to remove the photocatalyst and then monitored by a UNIC 7200 Apparatus UV-visible spectrophotometer at their maximum absorption wavelength. Total organic carbon (TOC) was carried out for selected samples to evaluate the degree of dye mineralization using a TOC analyzer (TOC-VCPH, Shimadzu).

Results and discussion

Zinc-nickel citrate hollow microspheres obtained from the resulting suspension after aged at room temperature for 6 h are employed as the precursor for the fabrication of NiO–ZnO composite hollow microspheres. The morphology of as-synthesized precursor was examined by SEM and TEM, as shown in Fig. 1. The low-magnification SEM image shows that the precursor is composed of dispersed microspheres with an average diameter of 1.4 μm (Fig. 1a). The SEM micrograph in the inset in Fig. 1a shows a broken sphere, providing evidence of a hollow structure. The high-magnification SEM micrograph exhibits that the surface of the microsphere is quite rough and loose as shown in Fig. 1b. The TEM images (Fig. 1c and d) further confirm that the as-prepared precursors have a hollow structure. The thickness of the shell is about 300 nm. Energy dispersive spectroscopy (EDS) microanalysis of the precursor shows a Ni/Zn ratio of about 0.54 in Fig. S1 (ESI†). The XRD pattern of as-synthesized precursor (Fig. 2a) demonstrates that these hollow microspheres are mainly amorphous. Two weak diffraction peaks at around 33.3° and 59.8° (2θ) are attributed to some crystalline zinc citrate particles formed in the original preparation process of zinc citrate hollow microspheres as confirmed in our previous literature.[40] The as-prepared precursor is further investigated by FT-IR spectroscopy as shown in Fig. 2b. The IR spectra exhibit two intense absorption bands at 1586 cm^{-1} and 1404 cm^{-1}, which can be attributed to the antisymmetric and symmetric stretching vibrations for the carboxylate groups of the coordinated citrates, respectively. Both of the bands shift to lower frequencies compared with free citric acid, suggesting complexation to metal ions.[40–42] The typical absorption bands between 1700 and 1710 cm^{-1} arising from

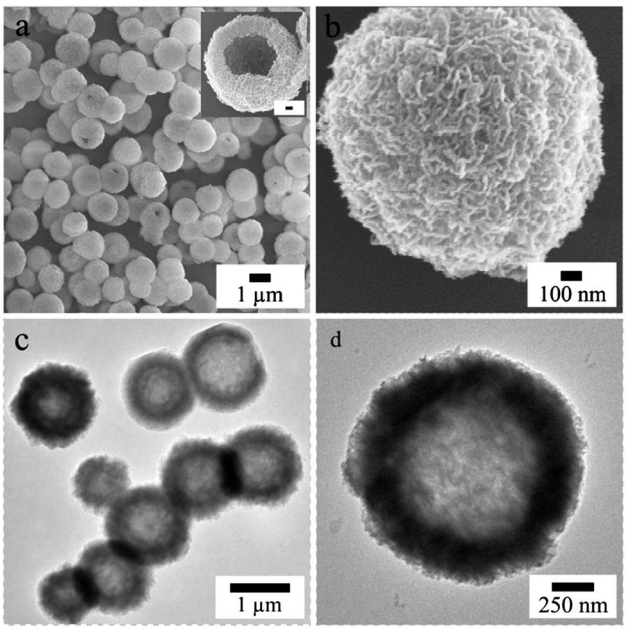

Fig. 1 (a) The SEM micrograph of the zinc-nickel citrate hollow microspheres obtained from the reaction solution aged at room temperature for 6 h. The inset shows a broken microsphere. (b) The higher magnification SEM image of an individual microsphere. (c) The low magnification TEM micrograph of the zinc-nickel citrate hollow microspheres. (d) The high magnification TEM micrograph of an individual microsphere. The scale bar in the inset represents 100 nm.

undissociated carboxylic acid groups could not be observed, which demonstrates that each carboxylic acid group is deprotonated.[42–44] The strong peaks at 3438 cm^{-1} can be ascribed to the vibrations of –OH groups for absorbed water. The typical survey XPS spectrum of the precursor is shown in Fig. 3a, which confirms the presence of Zn, Ni, O, and C elements. Fig. 3b shows the high-resolution Ni 2p spectrum, which can be deconvoluted into five peaks. The binding energies located at 853.9, 855.9, and 861.3 eV are ascribed to the Ni 2p3/2 peaks, while those centred at 872.6 and 879.5 eV are due to the Ni 2p1/2 peaks, indicating the presence of Ni^{2+} ions in the precursor.[45] Fig. 3c displays the high-resolution Zn 2p spectrum. Two major peaks at 1044.9 and 1021.9 eV correspond to the Zn $2p_{3/2}$ and Zn $2p_{1/2}$ energy levels, respectively.

The influence of ageing time on the morphology and component of the as-obtained zinc-nickel citrate was investigated. A series of experiments were performed with different ageing times, but with other synthesis parameters unchanged. As shown in Fig. S2 (ESI†), the molar ratio of Ni/Zn in the precursor increases from 0.37, 0.46, 0.541 to 0.548 with increasing the ageing time ranging from 1 h, 3 h, 6 h to 8 h. It can be further found that when the ageing time increases from 6 h to 8 h the molar ratio of Ni/Zn in the precursor remain almost unchanged, indicating that the adsorption amount of nickel ion on the surfaces of zinc citrate hollow microspheres reaches a maximum as the ageing time increases to 6 h. It is worth noting that the surfaces of zinc citrate hollow microspheres are rich in functional groups, such as –OH and $–COO^-$, available for metal ion adsorption, which is similar to the carbonaceous particles reported earlier.[46,47] When zinc citrate hollow microspheres were dispersed into nickel nitrate solution, nickel ions would adsorb on the rough and loose surfaces of zinc citrate hollow microspheres through coordination or electrostatic interactions between nickel ions and surface functional groups. The adsorption amount of nickel ion increases with the increase of ageing time and then reaches saturation when the ageing time increases to 6 h. A longer ageing time (>6 h) does not increase the content of nickel ion in the zinc-nickel citrate. Additionally, the surface hydrophilic groups can also serve as anchors to immobilize Ni^{2+} ions on the surface of the zinc citrate hollow microspheres, which can prevent them from aggregating and provide an excellent interface contact between NiO and ZnO in the subsequent calcination process.[47] As a result, it is beneficial for the formation of well-dispersed composite hollow microspheres and then enhances the photocatalytic activity.

Thermogravimetric analysis was performed to further characterize the thermal properties of zinc-nickel citrate hollow microspheres obtained from the reaction solution aged at room temperature for 6 h (Fig. S4, ESI†). A gradual weight loss at temperature below 290 °C is due to the dehydration of physically adsorbed water. The weight loss from 300 to 370 °C, corresponding to a mass loss of 45.8%, is attributed to the decomposition of zinc-nickel citrate to NiO–ZnO composites. The amorphous zinc-nickel citrate hollow microspheres

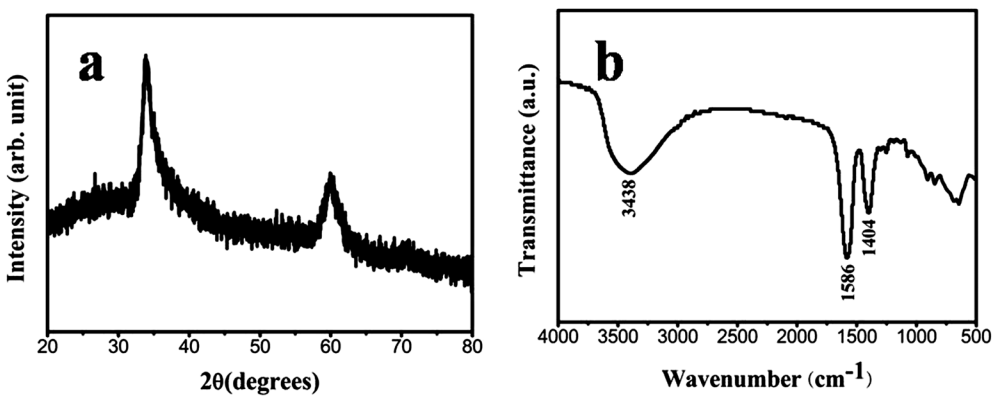

Fig. 2 (a) XRD pattern and (b) FT-IR spectrum of the zinc-nickel citrate hollow microspheres.

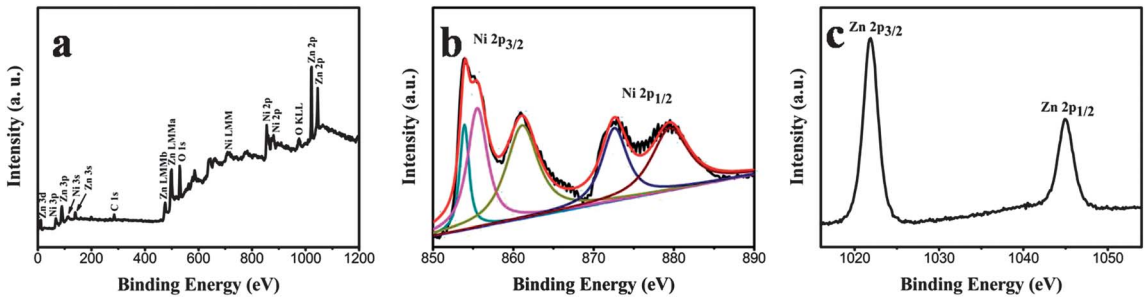

Fig. 3 XPS spectra for the zinc-nickel citrate hollow microspheres: (a) survey spectrum and high-resolution (b) Ni 2p and (c) Zn 2p spectra.

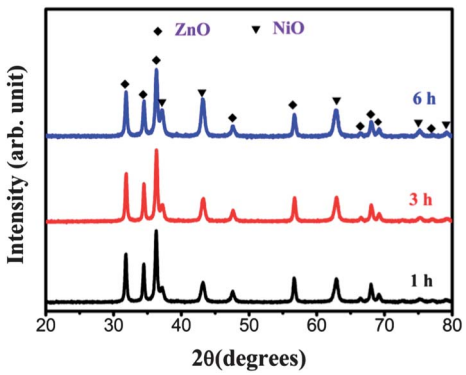

Fig. 4 The XRD patterns of the NiO–ZnO composite hollow microspheres calcinated from zinc-nickel citrate with different contents of nickel ions.

completely transform into crystalline NiO–ZnO composite hollow microspheres as the temperature further increases.

The as-obtained products after calcination of zinc-nickel citrate with different contents of nickel ions at 500 °C for 2 h were characterized by XRD to identify their crystal phases. As shown in Fig. 4, the diffraction peaks marked by quadrilaterals correspond to hexagonal ZnO (JCPDS card no. 36-1451) and those marked by triangles can be indexed to the cubic structure for NiO (JCPDS-78-0643). In addition, the intensity of diffraction peaks for NiO was improved gradually when increasing the content of nickel ion in the zinc-nickel citrate. No characteristic peaks for impurity are detectable. The strong and sharp peaks of NiO and ZnO exhibit the high crystallinity of the obtained NiO–ZnO composite hollow microspheres after calcining at 500 °C for 2 h. From the XRD pattern of NiO–ZnO composite hollow microspheres with the aging time of 6 h, the mean grain size of the ZnO and NiO particles were calculated to be about 26.5 and 27 nm, respectively, using the scherrer equation. In the following discussion, the NiO–ZnO composite microspheres prepared with the original ageing time of 1 h, 3 h and 6 h were denoted as NZ1, NZ3 and NZ6, respectively.

The morphology and the microstructure of the NZ6 were further investigated by SEM and TEM. As shown in Fig. 5, the product consists of dispersed hollow microspheres, which reveals that the NiO–ZnO composite microstructures have perfectly inherited the morphology of the zinc-nickel citrate structure after calcination. The average diameter of the NiO–ZnO composite hollow microspheres is 1.1 μm, implying that the microspheres shrink during the transformation from zinc-nickel citrate to NiO–ZnO composites. The SEM micrograph (the inset in Fig. 5a) displays a broken sphere, and the hollow structure can be easily discerned. The SEM image with a high magnification in Fig. 5b exhibits that the shells of the NiO–ZnO composite hollow microspheres consist of many nanoparticles with an average size of 30 nm, which is in accordance with the XRD results. NiO and ZnO nanoparticles connect intimately with each other, leading to the large and excellent contact interface between NiO and ZnO, which is beneficial for the transfer of photogenerated charge carriers. From the TEM observation shown in Fig. 5c, the contrast difference between the darker marginal region and the brighter central region further suggests the hollow structure of the obtained NiO–ZnO composite microspheres, which is in consistent with the SEM observations. The average thickness of the shell is about 200 nm. The HRTEM image (Fig. 5d) recorded from the circled region indicated by an arrow in Fig. 5c reveals the simultaneous presence of the lattice fringes belonging to crystalline ZnO and NiO. The interplanar distances of 0.26 nm are attributed to the lattice spacing of the (002) planes of the hexagonal structured ZnO while the interplanar distances of 0.21 nm agree well with the *d* spacings of the (200) planes of the cubic structured NiO. The molar ratios of Ni/Zn for NZ1, NZ3 and NZ6 are almost unchanged in comparison with their precursors, respectively (Fig. S3, ESI†). High-angle annular dark-field (HAADF) scanning TEM (STEM) image and elemental maps of Ni and Zn for NZ6 are shown in Fig. 5e–g, respectively. It can be clearly observed that the NiO and ZnO have homogeneous distribution in the shell of the composite hollow microspheres. These microscopic results suggest that the present method in this study leads to a well-dispersed mixed metal oxide hollow spheres without the formation of the large individual component aggregates. In addition, the coupling metal oxides contact closely, which is beneficial for fast charge transport at the interface and therefore facilitate the separation of the photogenerated electron–hole pairs. The textural feature of NZ6 composite hollow microspheres was further evaluated by nitrogen sorption measurement at 77 K. As depicted in Fig. 6, the Brunauer–Emmett–Teller (BET) surface area of the composite hollow microspheres is about 21.3 $m^2 g^{-1}$. The pore size distribution spectrum (the inset in Fig. 6) obtained from the Barrett–Joyner–Halenda method demonstrates a main pore size of about 11 nm.

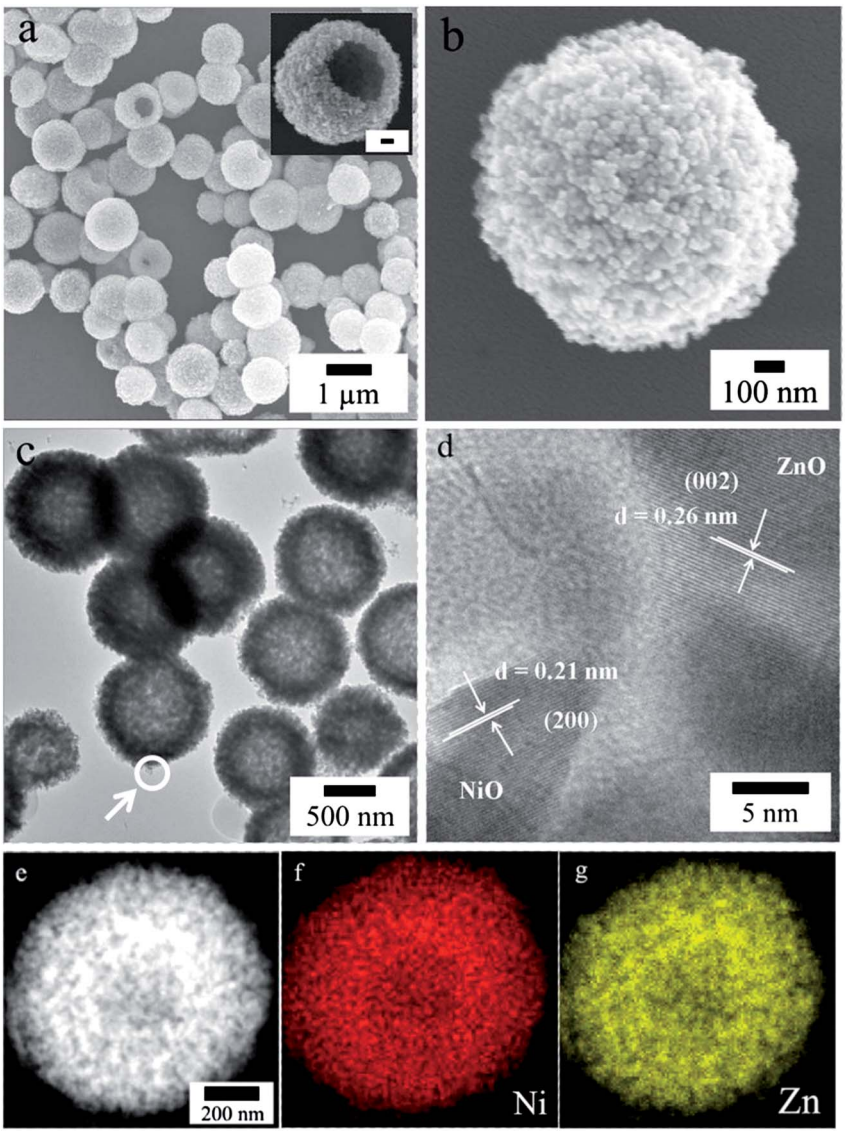

Fig. 5 (a) The low magnification SEM image of the NiO–ZnO composite hollow microspheres (NZ6). The inset shows a broken microsphere. (b) The high magnification SEM image of an individual microsphere. (c) The TEM image of the NiO–ZnO composite hollow microspheres. (d) The HRTEM micrograph of the shell area indicated by an arrow and a circle in (c). (e) HAADF image of a microsphere. (f) Elemental mapping of Ni. (g) Elemental mapping of Zn. The scale bar in the inset represents 100 nm.

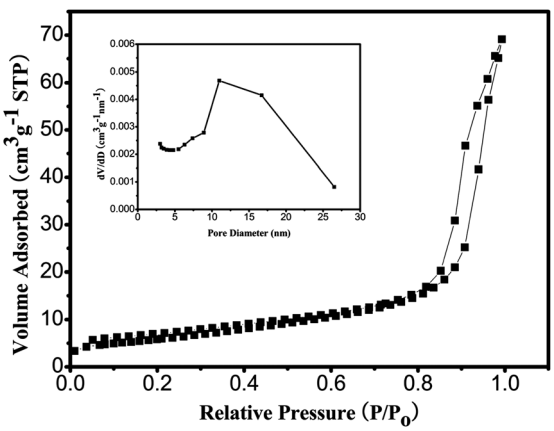

Fig. 6 N_2 adsorption–desorption isotherm of the NZ6 composite hollow microspheres. The inset shows the corresponding pore size distribution.

Fig. 7 illustrates the UV-visible absorption spectra for ZnO, NZ1, NZ3 and NZ6 hollow microspheres. For comparison, ZnO hollow microspheres were prepared by calcining the original zinc citrate hollow microspheres at 500 °C for 2 h without ageing at nickel nitrate solution. NZ1, NZ3 and NZ6 composites all exhibit absorption in both UV and visible region, compared to only absorption in the UV region with ZnO hollow microspheres. Moreover, the absorption intensity for the visible light improves with increasing the content of NiO in the composites. These results imply that the as-prepared NiO–ZnO composite hollow microspheres have optical capability nearly in the whole range of visible light region. The enhanced absorbance at the range of 400–800 nm may be attributed to the synergetic effect between ZnO and NiO, implying the excellent interfacial interaction.

Different organic dyes including RhB, MB and MO were used as model pollutants to evaluate the photocatalytic activities of

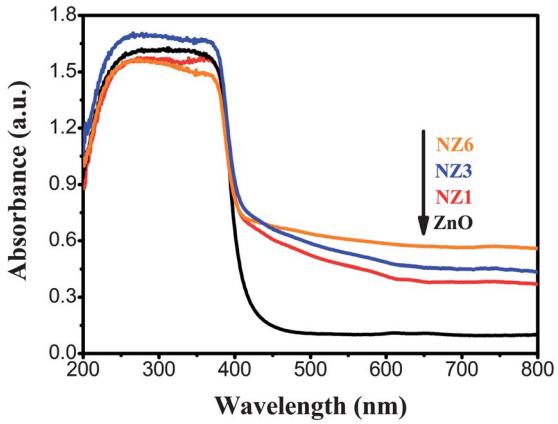

Fig. 7 UV-visible absorption spectra of ZnO, NZ1, NZ3 and NZ6 composite hollow microspheres.

the as-produced NiO–ZnO composites under UV irradiation. The influence of photocatalyst weight and initial dye concentration on the photocatalytic efficiency were investigated in order to find out the optimal photocatalytic parameters. Firstly, 10 mg L^{-1} RhB (200 mL) and NZ6 hollow microspheres were used as the initial dye concentration and photocatalyst, respectively. The photocatalyst dosage ranges from 0.08, 0.12, 0.16 to 0.20 g. As displayed in Fig. S5 (ESI†), it can be found that the photocatalytic efficiency obviously increases when increasing the photocatalyst weight from 0.08 to 0.16 g under UV irradiation for 80 min. The photocatalytic efficiency decreases with further increase of photocatalyst weight from 0.16 to 0.20 g. This phenomenon could be elucidated in two aspects, including the availability of active sites and the penetration of UV light. Generally, the total active surface area would increase when increasing the catalyst dosage, leading to the initial increase of photocatalytic efficiency. However, when the catalyst dosage exceeds 0.16 g, UV light penetration in the solution significantly decreases due to the enhanced light scattering arose from the catalyst powders, giving rise to a decrease in photocatalytic efficiency. Thus, 0.16 g was determined to be the optimal dosage of photocatalyst. Secondly, the effect of initial RhB concentration on the photocatalytic efficiency was investigated in the range of 5–20 mg L^{-1} under UV irradiation for 80 min (Fig. S6, ESI†). The photocatalytic efficiency increases with the increase of RhB concentration from 5 to 10 mg L^{-1} and subsequently decreases with further increase of RhB concentration to 20 mg L^{-1}. More RhB molecules would adsorbed on the surface of NZ6 hollow microspheres when the initial dye concentration increases, which results in the improvement of photocatalytic efficiency. When the dye concentration exceeds 10 mg L^{-1}, the surface of NZ6 hollow microspheres were almost occupied by the excess RhB molecules, which is bad for the adsorption of hydroxyl ions and subsequent generation of hydroxyl radicals. Moreover,

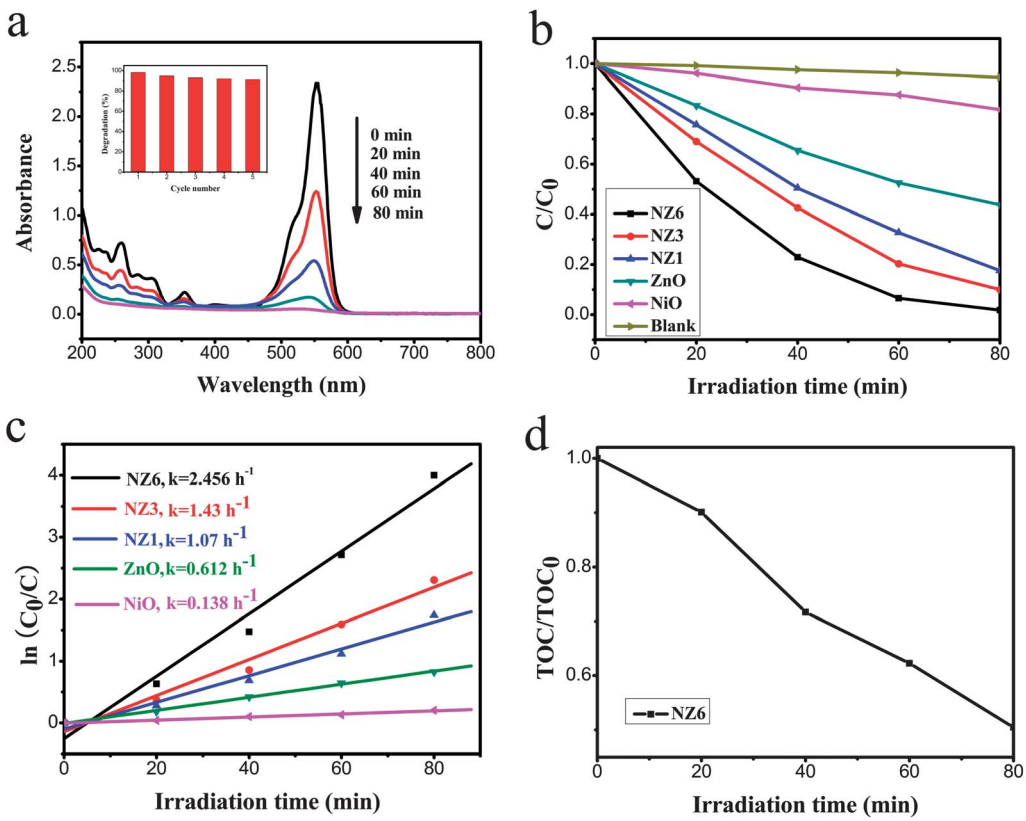

Fig. 8 (a) UV-vis spectra of the aqueous solutions of RhB after UV irradiation for different time periods in the presence of NZ6 hollow microspheres. (b) Photodegradation of RhB in the presence of NiO, ZnO, NZ1, NZ3 and NZ6, as well as in the absence of ZnO. (c) Kinetic linear simulation curves of RhB photocatalytic degradation. (d) TOC curves of photocatalytic degradation of RhB on NZ6 hollow microspheres during different time periods. The inset in (a) illustrates photocatalytic activity of the NZ6 hollow microspheres for RhB degradation with five cycles.

the excess dye substances would hinder the photons to reach the catalyst surface. Thus, the optical dye concentration is determined to be 10 mg L^{-1}. Based on the above experiments, 0.16 g of catalyst weight and 10 mg L^{-1} of initial dye concentration were deemed as the optical photocatalytic parameters and employed in the following photocatalytic reactions. As observed in Fig. 8a, the intensity of the characteristic absorption for RhB at 664 nm decreases gradually with increasing the irradiation time, demonstrating the photocatalytic degradation of RhB in the presence of NZ6 composite hollow microspheres. Fig. 8b shows the normalised RhB concentration in the RhB solution as a function of UV irradiation time in the presence of the NiO, ZnO, NZ1, NZ3 and NZ6 composite hollow microspheres. After a UV irradiation time of 80 min, 18.33%, 56%, 82%, 90% and 98% RhB was decomposed in the presence of NiO, ZnO, NZ1, NZ3 and NZ6, respectively. A comparative experiment in the absence of the photocatalyst during UV irradiation exhibits only 8% RhB decomposition (Fig. 8b). It can be observed that the photocatalysis efficiency gradually improves with increasing the content of NiO in the composites and the NZ6 exhibit the highest photocatalytic activity. The photocatalytic process complies with first-order kinetics, $c = c_0 \exp(-kt)$, where c is the RhB concentration after UV irradiation, c_0 is the initial RhB concentration, t is the UV irradiation time, and the constant k represents the reaction rate.[48] The kinetic linear simulation curves of RhB photodegradation with the samples of NiO, ZnO, NZ1, NZ3 and NZ6 are depicted in Fig. 8c. The reaction rates k for the NiO, ZnO, NZ1, NZ3 and NZ6 are calculated to be 0.138, 0.612, 1.072, 1.43 and 2.456 h^{-1} respectively. It suggests that the photocatalytic activity order was NZ6 > NZ3 > NZ1> ZnO > NiO, which was in accordance with the activity studies above. The degree of mineralization of RhB for NZ6 hollow microspheres during the photodegradation process was also investigated using the total organic carbon (TOC) methods and the results are displayed in Fig. 8d. It can be observed that the total mineralization is about 50.4% after 80 min illumination. This indicates that RhB decolorization is faster than the decrease of TOC, which may be ascribed to the gradual mineralization of RhB during the photocatalytic process. Fig. 9a and b reveal the degradation behavior of MB catalyzed by the photocatalysts under UV irradiation. Almost 98% of MB is decomposed using NZ6 composites after 60 min of irradiation, which is obviously higher than 59% of ZnO hollow microspheres. Similar to the kinetic study of photocatalytic degradation of RhB, the reaction rates k for the photocatalytic degradation of MB with NiO, ZnO, NZ1, NZ3 and NZ6 are determined to be 0.207, 0.99, 2.03, 2.83 and 3.99 h^{-1} respectively. TOC is reduced to 61.3% on NZ6 hollow microspheres after 60 min irradiation. Fig. 9c and d show the degradation behavior of MO photocatalyzed under UV illumination. It can be found that about 99.6% of MO can be photodegraded using NZ6 within 80 min. When used ZnO hollow microspheres as photocatalysts, only 60%

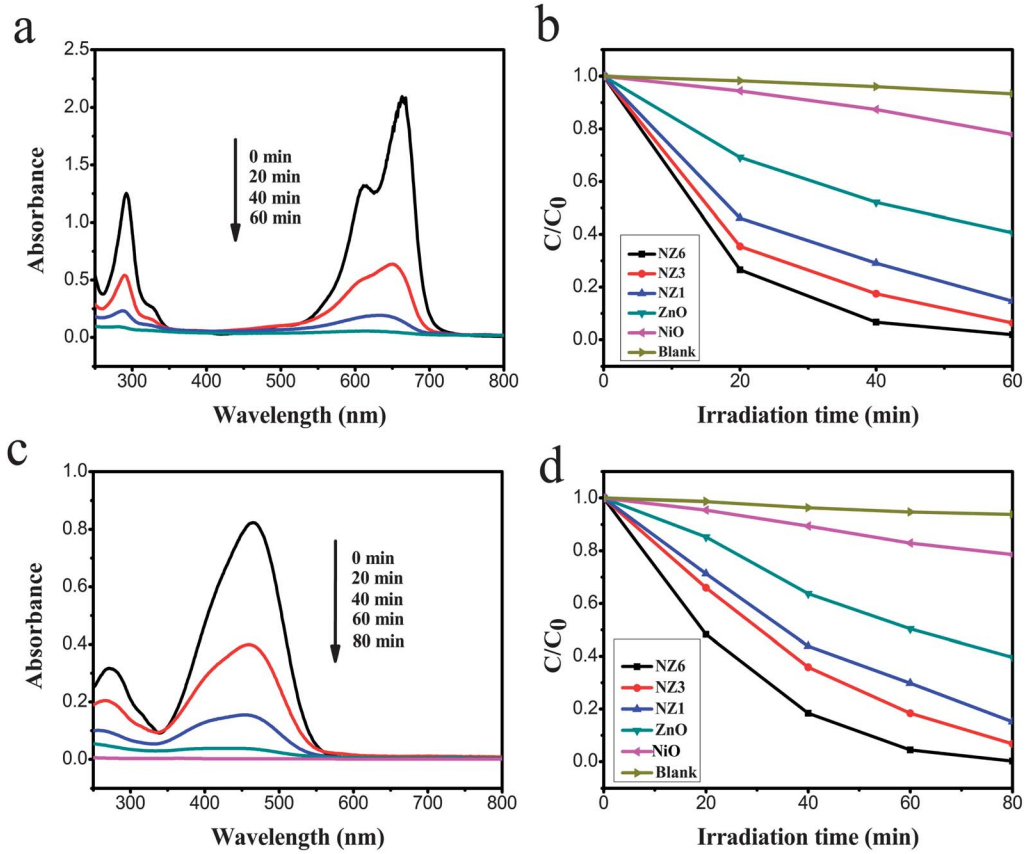

Fig. 9 UV-vis spectra of the aqueous solutions of MB (a) and MO (c) after UV irradiation for different time periods in the presence of NZ6 hollow microspheres. Photodegradation of MB (b) and MO (d) in the presence of NiO, ZnO, NZ1, NZ3 and NZ6, as well as in the absence of ZnO.

Table 1 Comparison of photocatalytic properties for NiO–ZnO composites with different morphologies and ZnO-based composites

Materials	Morphology	Dye	Degradation time (min)	Ref.
NiO–ZnO	Nanofibers	RhB	50	39
	Powders	MO	120	49
CeO_2–ZnO	Nanofibers	RhB	180	51
In_2O_3–ZnO	Nanoparticles	MB	120	50
CdS–ZnO	Hierarchical microspheres	RhB	200	52
	Nanoparticles–nanorods	MB	120	30
Fe_2O_3–ZnO	Hollow structures	RhB/MO/MB	>50/80/50	1
CdO–ZnO	Nanorods	MB	360	53
NiO–ZnO	Hollow microspheres	RhB/MO/MB	80/80/60	Our work

of MO can be degraded. Similar to the kinetic study of photocatalytic degradation of RhB, the reaction rates k for the photocatalytic degradation of MO with NiO, ZnO, NZ1, NZ3 and NZ6 are calculated to be 0.169, 0.63, 1.22, 1.62 and 3.13 h^{-1} respectively. TOC removal efficiency is about 54.4% on NZ6 hollow microspheres within 80 min. Consequently, NZ6 composite hollow microspheres show the highest photodegradation efficiency of the above dyes. Due to the different photocatalytic reaction conditions, a straightforward comparison of photocatalytic properties for different materials is usually difficult. However, it is well known that the photocatalytic properties of mixed metal oxides depend strong on their morphology, component and the interfacial interactions. Thus, a rough comparison of the photocatalytic efficiency for NiO–ZnO composites with different morphology and other heterojunction materials is employed and the results are listed in Table 1. For example, MO could be nearly decolorized for NZ6 hollow microspheres after 80 min of UV irradiation, compared to 120 min when using NiO–ZnO powders reported by Fornasiero.[49] Shao's group reported the successful preparation of NiO–ZnO nanofibers, which shows 1.3 times photocatalytic efficiency higher than pure ZnO nanofibers for the degradation of RhB.[39] In the present work, the photocatalytic efficiency of NZ6 with the similar composition for the degradation of RhB is 1.75 times higher than pure ZnO hollow microspheres. The improvement of photocatalytic efficiency for NZ6 composite hollow microspheres is greater than the NiO–ZnO nanofibers, which is attributed to the intimate contact interface of as-obtained NiO–ZnO composite hollow microspheres. Almost 97% of MB is photodegraded by In_2O_3–ZnO hybrid nanoparticles within 120 min under UV irradiation, compared to 60 min when using NZ6 hollow microspheres.[50] Based on the above analysis, the as-produced NZ6 hollow microspheres show the excellent photocatalytic performances and may be within the range of the most promising photocatalysts. Additionally, the reusability of the photocatalyst was also investigated. In this case, NZ6 composites were repeatedly used to degrade RhB under UV irradiation (the inset in Fig. 8a). The photocatalytic activity of NZ6 composites decreases slightly after five photocatalysis cycles, indicating the superior stability of the photocatalysts. Additionally, NZ6 composites after photocatalytic degradation of RhB for five cycles were collected and further investigated by SEM and TEM. From Fig. S7 (ESI†), it can be clearly seen that the hollow morphology of NZ6 composites are almost unchanged, suggesting excellent structural retention during the photocatalysis process. Therefore, the excellent photocatalytic activity and superior stability of NZ6 composite hollow microspheres make it a promising catalyst for industrial wastewater treatment.

Fig. 10 displays the PL spectra of ZnO, NZ1, NZ3 and NZ6 hollow microspheres. The near-band edge UV emission located at 380 nm can be ascribed to the recombination of free excitons. The broad visible emissions ranging from 550 to 750 nm corresponds to the deep level of the trap-state emission of ZnO. Compared to pure ZnO hollow microspheres, the NiO–ZnO composite hollow microspheres depict much lower emission intensity. This phenomenon indicates that the recombination of the photogenerated electron–hole pairs was significantly suppressed in the NiO–ZnO composites.[39] Moreover, it can be found that the emission intensity of the NiO–ZnO composites decreases with increasing the loading amounts of NiO in the composites. NZ6 composite hollow microspheres show the lowest emission intensity, indicating the highest separation efficiency of photogenerated electron–hole pairs. The prolonged lifetime of photogenerated electron–hole pairs through the effective charge separation would facilitate the interfacial charge transfer between NiO and ZnO, leading to the enhanced photocatalytic activity of the NiO–ZnO composites.

Based on the above experimental observations and analysis, a suggested schematic energy band representing the charge transfer process in the NiO–ZnO composites is illustrated in Fig. 11. During the photocatalytic process, the electron would be excited from VB to CB under the illumination of the UV light with photon energy equal to or higher than the band gaps of NiO and ZnO. As a result, the same amount of holes would be formed simultaneously in the VB. In this band gap configuration, the photogenerated electron in the CB of NiO could migrate to the CB of ZnO. At the same time, the photogenerated holes in the VB of ZnO could conversely move to the VB of NiO. Moreover, the intimate contact interface of as-obtained NiO–ZnO composites strengthens the interfacial charge transport.

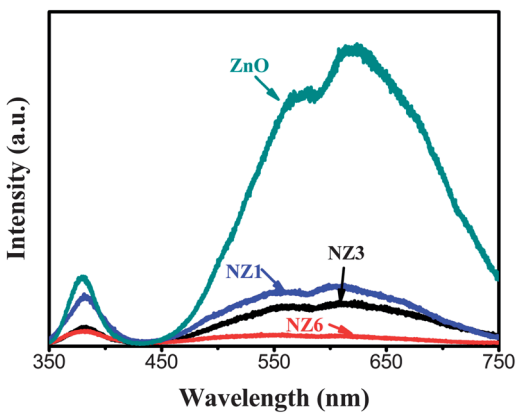

Fig. 10 The photoluminescence spectra of ZnO, NZ1, NZ3 and NZ6 composite hollow microspheres.

Therefore, the separation efficiency of photogenerated electron–hole pairs was significantly strengthened, which leading to the enhanced photocatalytic activity. Additionally, the more electrons and holes would migrate between ZnO and NiO with the increase of the content of NiO. Thus, NZ6 composite hollow microspheres with the highest content of NiO possess the highest photocatalytic activity. The possible photocatalytic reaction in our experiment is classified as follows:[39]

$$NiO–ZnO + h\nu \rightarrow e^- (ZnO) + h^+ (NiO)$$

$$e^- + O_2 \rightarrow \cdot O_2^-$$

$$h^+ + OH^- \rightarrow \cdot OH$$

$$\cdot O_2^- + H_2O \rightarrow \cdot O_2H + OH^-$$

$$\cdot O_2H + H_2O \rightarrow H_2O_2 + \cdot OH$$

$$H_2O_2 \rightarrow 2\cdot OH$$

$$\cdot OH + \text{dyes} \rightarrow CO_2 + H_2O$$

The hydroxyl radical species (·OH) would be produced through the reaction between the photogenerated holes and surface hydroxyl groups or H_2O at the catalyst surface. At the same time, the electrons were immediately trapped by the dissolved oxygen to form superoxide radical anions ($\cdot O_2^-$). Subsequently, the hydroperoxy radicals ($\cdot O_2H$) would be generated due to the protonation of superoxide radical anions ($\cdot O_2^-$), followed by the formation of hydroxyl radical species (·OH). The hydroxyl radical species (·OH) was an extremely strong oxidizing species which could effectively photodegrade the organic pollutants.[54,55] It is worth mentioning that this facile preparation method in our work can be employed to fabricate other ZnO-based composite hollow microspheres, such as CeO_2–ZnO and CdO–ZnO composite hollow microspheres. From the SEM and TEM images (Fig. S8, ESI†), it can be clearly observed that the as-obtained CeO_2–ZnO composites are composed of dispersed hollow microspheres. Energy dispersive spectroscopy (EDS) microanalysis (Fig. S9, ESI†) shows that the content of Ce increases from 33.3% to 50.0% with the increase of the ageing time from 30 to 60 min. As displayed in Fig. S10 (ESI†), CdO–ZnO composite hollow microspheres can also be prepared through this strategy and the content of Cd could also be adjusted simply by changing the ageing time. Other ZnO-based composite hollow microspheres that can be synthesized by this route are in progress.

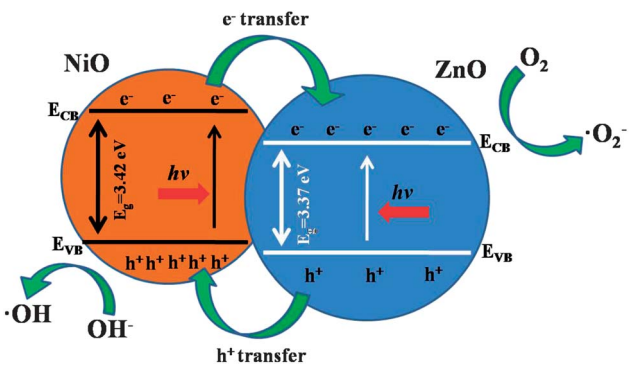

Fig. 11 Schematic of the energy band structure in NiO–ZnO composites.

Conclusions

In summary, amorphous zinc-nickel citrate hollow microspheres were successfully prepared through a novel, facile and template-free route. The molar ratios of Ni to Zn in the zinc-nickel citrate can be adjusted by simply changing the ageing time at nickel nitrate solution. After the calcination of the precursors at 500 °C for 2 h, the well-dispersed NiO–ZnO composite hollow microspheres with different content of NiO are synthesized for the first time. The optical absorption of NiO–ZnO composites extends to the visible region. The photocatalysis efficiencies for the degradation of different organic dyes including RhB, MB and MO under UV light irradiation gradually improve with increasing the content of NiO in the composites and the NZ6 composite hollow microspheres possess the highest photocatalytic activity. This synthesis method is highlighted by its simplicity, low cost, template-free and high-yield production, which may find important applications in the degradation of organic pollutant from wastewater and could also be used to synthesize other ZnO-based composite hollow microspheres, including CeO_2–ZnO and CdO–ZnO composite hollow microspheres.

Acknowledgements

The authors gratefully acknowledge financial support from the National Basic Research Program of China (no. 2012CB933103), the National Outstanding Youth Science Foundation of China (Grant no. 50825101), and the National Natural Science Foundation of China (Grant no. 51171158 and 50971108).

References

1 Y. Liu, L. Yu, Y. Hu, C. F. Guo, F. M. Zhang and X. W. Lou, *Nanoscale*, 2012, **4**, 183–187.
2 J. Kim, Y. Piao and T. Hyeon, *Chem. Soc. Rev.*, 2009, **38**, 372–390.
3 X. W. Lou, L. A. Archer and Z. C. Yang, *Adv. Mater.*, 2008, **20**, 3987–4019.
4 X. Y. Lai, J. E. Halpert and D. Wang, *Energy Environ. Sci.*, 2012, **5**, 5604–5618.
5 J. Hu, M. Chen, X. S. Fang and L. M. Wu, *Chem. Soc. Rev.*, 2011, **40**, 5472–5491.
6 L. Zhou, D. Zhao and X. W. Lou, *Adv. Mater.*, 2012, **24**, 745–748.
7 J. Liu, S. B. Hartono, Y. G. Jin, Z. Li, G. Q. M. Lu and S. Z. Qiao, *J. Mater. Chem.*, 2010, **20**, 4595–4601.
8 X. Wang, X. L. Wu, Y. G. Guo, Y. Zhong, X. Cao, Y. Ma and J. Yao, *Adv. Funct. Mater.*, 2010, **20**, 1680–1686.
9 J. Guan, F. Mou, Z. Sun and W. Shi, *Chem. Commun.*, 2010, **46**, 6605–6607.

10 X. Yu, C. Cao, H. Zhu, Q. Li, C. Liu and Q. Gong, *Adv. Funct. Mater.*, 2007, **17**, 1397–1401.
11 J. Liu, S. Z. Qiao, J. S. Chen, X. W. Lou, X. Lu and G. Q. Xing, *Chem. Commun.*, 2011, **47**, 12578–12591.
12 F. Niu, A. M. Cao, W. G. Song and L. J. Wan, *J. Phys. Chem. C*, 2008, **112**, 17988–17993.
13 H. J. Fan, U. Gösele and M. Zacharias, *Small*, 2007, **3**, 1660–1671.
14 Y. J. Xiong, B. Wiley, J. Y. Chen, Z. Y. Li, Y. D. Yin and Y. N. Xia, *Angew. Chem., Int. Ed.*, 2005, **44**, 7913–7917.
15 E. C. Cho, P. H. C. Camargo and Y. N. Xia, *Adv. Mater.*, 2010, **22**, 744–748.
16 X. Z. Gong, Y. Yang and S. M. Huang, *J. Phys. Chem. C*, 2010, **114**, 18073–18080.
17 D. Chen, H. Zhang, S. Hu and J. Li, *J. Phys. Chem. C*, 2008, **112**, 117–122.
18 S. S. Warule, N. S. Chaudhari, B. B. Kale, K. R. Patil, P. M. Koinkar, M. A. More and R. Murakamie, *J. Mater. Chem.*, 2012, **22**, 8887–8895.
19 T. Y. Ma, Z. Y. Yuan and J. L. Cao, *Eur. J. Inorg. Chem.*, 2010, **5**, 716–724.
20 M. Agrawal, S. Gupta, A. Pich, N. E. Zafeiropoulos and M. Stamm, *Chem. Mater.*, 2009, **21**, 5343–5348.
21 E. S. Jang, J. H. Won, S. J. Hwang and J. H. Choy, *Adv. Mater.*, 2006, **18**, 3309–3312.
22 Z. L. Wang, *ACS Nano*, 2008, **2**, 1987–1992.
23 A. Mclaren, T. Valdes-Solis, G. Li and S. C. Tsang, *J. Am. Chem. Soc.*, 2009, **131**, 12540–12541.
24 L. Xu, Y. Hu, C. Pelligra, C. Chen, L. Jin, H. Huang, S. Sithambaram, M. Aindow, R. Joesten and S. L. Suib, *Chem. Mater.*, 2009, **21**, 2875–2885.
25 D. W. Chu, Y. Masuda, T. Ohji and K. Kato, *Langmuir*, 2010, **26**, 2811–2815.
26 B. X. Li and Y. F. Wang, *J. Phys. Chem. C*, 2010, **114**, 890–896.
27 T. J. Kuo, C. N. Lin, C. L. Kuo and M. H. Huang, *Chem. Mater.*, 2007, **19**, 5143–5147.
28 L. Y. Yang, S. Y. Dong, J. H. Sun, J. L. Feng, Q. H. Wu and S. P. Sun, *J. Hazard. Mater.*, 2010, **179**, 438–443.
29 Z. Y. Zhang, C. L. Shao, X. H. Li, L. Zhang, H. M. Xue, C. H. Wang and Y. C. Liu, *J. Phys. Chem. C*, 2010, **114**, 7920–7925.
30 P. Kundu, P. A. Deshpande, G. Madras and N. Ravishankar, *J. Mater. Chem.*, 2011, **21**, 4209–4216.
31 L. R. Zheng, Y. H. Zheng, C. Q. Chen, Y. Y. Zhan, X. Y. Lin, Q. Zheng, K. M. Wei and J. F. Zhu, *Inorg. Chem.*, 2009, **48**, 1819–1825.
32 Y. Hu, H. H. Qian, Y. Liu, G. H. Du, F. M. Zhang, L. B. Wang and X. Hu, *CrystEngComm*, 2011, **13**, 3438–3443.
33 T. L. Lai, C. C. Lee, G. L. Huang, Y. Y. Shu and C. B. Wang, *Appl. Catal., B*, 2008, **78**, 151–157.
34 I. Hotovy, J. Huran, L. Spiess, S. Hascik and V. Rehacek, *Sens. Actuators, B*, 1999, **57**, 147–152.
35 J. L. Garcia-Miquel, Q. Zhang, S. J. Allen, A. Rougier, A. Blyr, H. O. Davies, A. C. Jones, T. J. Leedham, P. A. Williams and S. A. Impey, *Thin Solid Films*, 2003, **424**, 165–170.
36 M. Borgstrom, E. Blart, G. Boschloo, E. Mukhtar, A. Hagfeldt, L. Hammarstrom and F. Odobel, *J. Phys. Chem. B*, 2005, **109**, 22928–22934.
37 H. Ohta, M. Hirano, K. Nakahara, H. Maruta, T. Tanabe, M. Kamiya, T. Kamiya and H. Hosono, *Appl. Phys. Lett.*, 2003, **83**, 1029–1031.
38 J. Y. Wang, C. Y. Lee, Y. T. Chen, C. T. Chen, Y. L. Chen, C. F. Lin and Y. F. Chen, *Appl. Phys. Lett.*, 2009, **95**, 131117–131119.
39 Z. Y. Zhang, C. L. Shao, X. H. Li, C. H. Wang, M. Y. Zhang and Y. C. Liu, *ACS Appl. Mater. Interfaces*, 2010, **2**, 2915–2923.
40 Q. S. Xie, J. G. Li, Q. Tian and R. R. Shi, *J. Mater. Chem.*, 2012, **22**, 13541–13547.
41 S. Cho, J. W. Jang, A. Jung, S. H. Lee, J. Lee, J. S. Lee and K. H. Lee, *Langmuir*, 2011, **27**, 371–378.
42 P. Che, D. Fang, D. Zhang, J. Feng, J. Wang, N. Hu and J. Meng, *J. Coord. Chem.*, 2005, **58**, 1581–1588.
43 M. M. Milanova, M. G. Arnaudov, M. M. Getsova and D. S. Todorovsky, *J. Alloys Compd.*, 1998, **264**, 95–103.
44 K. D. Demadis and D. Coucouvanis, *Inorg. Chem.*, 1995, **34**, 436–448.
45 B. Zhao, X. K. Ke, J. H. Bao, C. L. Wang, L. Dong, Y. W. Chen and H. L. Chen, *J. Phys. Chem. C*, 2009, **113**, 14440–14447.
46 X. Y. Lai, J. Li, B. A. Korgel, Z. H. Dong, Z. M. Li, F. B. Su, J. Du and D. Wang, *Angew. Chem., Int. Ed.*, 2011, **50**, 2738–2741.
47 M. J. Zhou, Y. Hu, Y. Liu, W. L. Yang and H. S. Qian, *CrystEngComm*, 2012, **14**, 7686–7693.
48 N. V. Kaneva, G. G. Yordanov and C. D. Dushkin, *React. Kinet. Catal. Lett.*, 2009, **98**, 259–263.
49 A. Hameed, T. Montini, V. Gombac and P. Fornasiero, *Photochem. Photobiol. Sci.*, 2009, **8**, 677–682.
50 Z. Y. Wang, B. B. Huang, Y. Dai, X. Y. Qin, X. Y. Zhang, P. Wang, H. X. Liu and J. X. Yu, *J. Phys. Chem. C*, 2009, **113**, 4612–4617.
51 C. R. Li, R. Chen, X. Q. Zhang, S. X. Shu, J. Xiong, Y. Y. Zheng and W. J. Dong, *Mater. Lett.*, 2011, **65**, 1327–1330.
52 F. Xu, Y. F. Yuan, H. J. Han, D. P. Wu, Z. Y. Gao and K. Jiang, *CrystEngComm*, 2012, **14**, 3615–3622.
53 R. Saravanan, H. Shankar, T. Prakash, V. Narayanan and A. Stephen, *Mater. Chem. Phys.*, 2011, **125**, 277–280.
54 T. Aarthi and G. Madras, *Ind. Eng. Chem. Res.*, 2007, **46**, 7–14.
55 K. Rajeshwar, M. E. Osugi, W. Chanmanee, C. R. Chenthamarakshan, M. V. B. Zanoni, P. Kajitvichyanukul and R. Krishnan-Ayer, *J. Photochem. Photobiol., C*, 2008, **9**, 171–192.